THY-Tau22 mouse model accumulates more tauopathy at late stage of the disease in response to microglia deactivation through TREM2 deficiency

Audrey Vautheny, Charlotte Duwat, Gwennaëlle Aurégan, Charlène Joséphine, Anne-Sophie Hérard, Caroline Jan, Julien Mitja, Pauline Gipchtein, Marie-Claude Gaillard, Luc Buée, et al.

Neurobiology of Disease 155 (2021) 105398

Contents lists available at ScienceDirect

Neurobiology of Disease

journal homepage: www.elsevier.com/locate/ynbdi

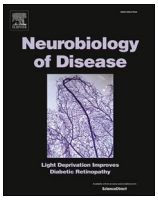

THY-Tau22 mouse model accumulates more tauopathy at late stage of the disease in response to microglia deactivation through TREM2 deficiency

Audrey Vautheny [a,1], Charlotte Duwat [a,1], Gwennaëlle Aurégan [a], Charlène Joséphine [a], Anne-Sophie Hérard [a], Caroline Jan [a], Julien Mitja [a], Pauline Gipchtein [a], Marie-Claude Gaillard [a], Luc Buée [b,c], David Blum [b,c], Philippe Hantraye [a], Gilles Bonvento [a], Emmanuel Brouillet [a], Karine Cambon [a], Alexis-Pierre Bemelmans [a,*]

[a] Université Paris-Saclay, CEA, CNRS, MIRCen, Laboratoire des Maladies Neurodégénératives, Fontenay-aux-Roses, France
[b] University of Lille, Inserm, CHU Lille, U1172 LilNCog - Lille Neuroscience & Cognition, Lille, France
[c] Alzheimer and Tauopathies, LabEx DISTALZ, France

ARTICLE INFO

Keywords:
Tauopathy
Microglia
Trem2
Animal model

ABSTRACT

The role played by microglia has taken the center of the stage in the etiology of Alzheimer's disease (AD). Several genome-wide association studies carried out on large cohorts of patients have indeed revealed a large number of genetic susceptibility factors corresponding to genes involved in neuroinflammation and expressed specifically by microglia in the brain. Among these genes *TREM2*, a cell surface receptor expressed by microglia, arouses strong interest because its R47H variant confers a risk of developing AD comparable to the ε4 allele of the *APOE* gene. Since this discovery, a growing number of studies have therefore examined the role played by TREM2 in the evolution of amyloid plaques and neurofibrillary tangles, the two brain lesions characteristic of AD. Many studies report conflicting results, reflecting the complex nature of microglial activation in AD. Here, we investigated the impact of TREM2 deficiency in the THY-Tau22 transgenic line, a well-characterized model of tauopathy. Our study reports an increase in the severity of tauopathy lesions in mice deficient in TREM2 occurring at an advanced stage of the pathology. This exacerbation of pathology was associated with a reduction in microglial activation indicated by typical morphological features and altered expression of specific markers. However, it was not accompanied by any further changes in memory performance. Our longitudinal study confirms that a defect in microglial TREM2 signaling leads to an increase in neuronal tauopathy occurring only at late stages of the disease.

1. Introduction

Alzheimer's disease (AD) is a progressive neurodegenerative disease and the most common cause of dementia worldwide with more than 35 million people affected (World Health Organization, Global action plan on the public health response to dementia 2017–2025), and about 6 million people in the USA only (Hebert et al., 2013). AD is characterized by two pathological lesions that are always associated in the patients' brains: extracellular accumulation of senile plaques made of β-amyloid peptide deposits, and neurofibrillary tangles (NFTs) formed by the intraneuronal aggregation of hyperphosphorylated Tau proteins (Serrano-Pozo et al., 2011). These lesions are associated with neuroinflammatory processes involving astrocytic and microglial activation (Webers, 2019). Several genetic studies conducted in recent years on large cohorts of patients have identified numerous risk factors related to genes specifically expressed in microglia, the resident immune cells of the central nervous system. The *TREM2* gene has focused particular attention because some of its polymorphisms, although rarely present in the general population, confer a risk of developing AD comparable to ε4 allele of the ApoE gene (Guerreiro et al., 2013; Jonsson et al., 2013). TREM2 is specifically expressed by the myeloid lineage (Bouchon et al., 2001; Turnbull et al., 2006), which is represented by microglial cells in the brain. In the case of AD, concentration and activation of microglia around amyloid plaques have been consistently observed, as originally

* Corresponding author at: MIRCen / CEA, 18 route du Panorama, F-92265 Fontenay-aux-Roses, France.
E-mail address: alexis.bemelmans@cea.fr (A.-P. Bemelmans).
[1] AV and CD contributed equally to this work.

https://doi.org/10.1016/j.nbd.2021.105398
Received 19 February 2021; Received in revised form 27 April 2021; Accepted 16 May 2021
Available online 18 May 2021

demonstrated by Alois Alzheimer (Cipriani et al., 2011). Consequently, pan-genomic studies demonstrating the involvement of TREM2 were rapidly followed by experimental studies aimed at elucidating its role in amyloid models of the disease. The first published studies, on different models, reported conflicting results. Indeed, Wang et al. demonstrated that the invalidation of *Trem2* caused an increased amyloid load in pathologically advanced 5xFAD mice (Wang et al., 2015), while Jay et al. reported that *Trem2* deficiency mitigated amyloid load in APPPS1–21 mice at the beginning of the pathology (Jay et al., 2015). A second study of this model at a later stage however demonstrated an increased in amyloid load (Jay et al., 2017), suggesting a versatile role of TREM2 depending on the stage of the pathology. More recently, single-cell RNAseq characterization of microglia in different AD models has shown the existence of a subpopulation of microglial cells associated to the pathology and whose activation is dependent on TREM2 (Keren-Shaul et al., 2017; Krasemann et al., 2017). This subpopulation, called DAM (disease-associated microglia) or MGnD (microglial neurodegenerative phenotype), may have a beneficial role by stimulating the phagocytic activity to phagocyte and contain the senile plaque in formation.

Number of studies now report a tight link between microglia and Tau pathology development (Ising, 2019; Laurent et al., 2018; Laurent et al., 2017), including Tau pathology seeding and spreading (Asai et al., 2015; Hopp et al., 2018; Maphis, 2015; Stancu et al., 2019). This prime role of microglia in Tau pathology development logically raised questions on the potential role that TREM2 receptor might play in the development of tauopathy. In a similar manner to amyloid models, several mouse models of tauopathy were crossed with TREM2 deficient mice. Using the PS19 model, which express the human 1N4R Tau form bearing the P301S mutation, Leyns et al. reported that TREM2 deficiency moderates microglial activation and neurodegeneration in these animals while the extent of tauopathy remained unchanged (Leyns et al., 2017). Similar results were reported in the same mice expressing the R47H variant of TREM2 (Gratuze et al., 2020). Puzzingly, the magnitude of TREM2 loss-of-function could promote differential outcomes (Sayed et al., 2018). In sharp contrast, using another transgenic model expressing the wild-type human Tau on a murine Tau knockout background, Bemiller et al. showed that *Trem2* deficiency leads on the contrary to an aggravation of tauopathy (Bemiller et al., 2017). Overall, data published to date on the role of TREM2 in tauopathy remain conflicting and need to be further investigated. In order to study the role of TREM2 at different stages of Tau pathology, we took advantage of the progressive THY-Tau22 model (Schindowski et al., 2006). This transgenic line over-expresses the human 1N4R Tau carrying the G272V and P301S mutations under the control of the Thy1.2 neuronal promoter, resulting in the development of hippocampal Tau pathology associated with synaptic, neuro-inflammatory and cognitive alterations that progressively evolve from 3 to 10–12 months of age (Chatterjee et al., 2018; Laurent et al., 2017; Van der Jeugd et al., 2011; Van der Jeugd et al., 2013a). In the present study, to appreciate the potential impact of Trem2 deficiency over the course of Tau pathology development, we deleted *Trem2* from THY-Tau22 mice and investigate outcome in a longitudinal study from an early stage (3 months), where pathology initiates, to a late stage (12 months), where pathology is fully developed. Overall, our data indicated that TREM2 deficiency dampened microglial activation and hippocampal atrophy while increasing tauopathy at late stages, suggestive of a complex role of TREM2 in tauopathy.

2. Material and methods

2.1. Animals

Animal procedures were performed in accordance with the French regulation (EU directive 86/609 – French Act Rural Code R214–87 to 131). The animal facility was approved by veterinarian inspections (authorization n° B92–032-02) and complied with Standards for Humane Care and Use of Laboratory Animals of the Office of Laboratory Animal Welfare.

(OLAW – n°#A5826-01). All procedures received approval from the local ethical committee (Comité d'Ethique en Expérimentation Animale CEA) and the French Ministry of Research (*APAFIS#612-2015,050,514,376,362 v3*). THY-Tau22 heterozygous mice (Schindowski et al., 2006) expressing the 412 amino acids isoform of human Tau with 4-repeat domains (1N4R) and bearing the G272V and P301S point-mutations, were crossed with $Trem2^{-/-}$ or $Trem2^{+/+}$ littermate mice (Turnbull et al., 2006) to generate $Trem2^{+/+}$*;Tau22* and $Trem2^{-/-}$*; Tau22* mice. Both males and females were used for analysis in this study. All mice were backcrossed on a C57BL/6J genetic background.

2.2. Immunohistology

Mice were anesthetized by intraperitoneal injection of a lethal dose of pentobarbital. Tissues were fixed by cardiac perfusion with 15 mL of 0.9% NaCl followed by 100 mL of 4% paraformaldehyde. Brains were then post-fixed for 24 h in the same fixative before being transferred in PBS containing 30% sucrose and stored at 4 °C until sectioning. Brains were cut coronally into 12 series of 30-μm thick sections on a freezing sliding microtome (SM1020R; LeicaTM) and stored in cryoprotectant solution at −20 °C until use.

For AT100, free-floating sections were incubated for 30 min with 0.3% H_2O_2 in PBS. After rinsing with 0.01 M PBS, 0.2% TritonX-100 (Sigma), sections were incubated 1 h in blocking solution containing 4% normal goat serum (NGS) in PBS and transferred into primary antibody solution for incubation overnight at 4 °C. After rinsing, sections were incubated with a goat anti-mouse IgG secondary antibody (1/1000 dilution into blocking solution) for 1 h at room temperature and revealed using Vectastain ABC Kit and a DAB substrate (Vector Laboratories) according to manufacturer's instructions. Sections were then mounted on slides and dehydrated in increasing ethanol concentrations and xylene before mounting using Eukitt (Dutscher, France).

For free-floating immunofluorescence, sections were incubated directly in blocking solution before transfer into primary antibody solutions for incubation overnight at +4 °C. After rinsing with 0.01 M PBS, sections were incubated for 1 h at RT into blocking solution containing 1/1000 Alexa-coupled secondary antibodies (Thermo Fisher). AT8 immunostaining was amplified using CY3-coupled streptavidin diluted to 1/1000 in blocking solution (Sigma-Aldrich). Sections were then mounted on slides with Mowiol. For primary antibody dilutions, see Supplementary Table 1.

For Gallyas silver impregnation sections were washed 3 times in sterile 0.1 M PBS, mounted on slides and left for drying overnight. Sections were then permeabilized by incubation into toluene followed by decreasing ethanol concentrations (100%, 90% and 70%). Slides were then transferred into a 0.25% potassium permanganate for 15 min, incubated 2 min in 2% oxalic acid followed by a 60 min incubation into a solution containing 0.4 g lanthanum nitrate, 2 g sodium acetate and 30% hydrogen peroxide in a volume of 100 mL. Slides were then rinsed 3 times with distilled water before incubation for 2 min in a solution containing 0.035% AgNO3, 0.04 g/mL of NaOH and 0.1 g/mL KI. Reaction was then stopped by rinsing with 0.5% acetic acid and development performed by incubation for 20 min in a solution containing 2 g/L NH4NO3, 2 g/L AgNO3, 10 g/L tungstosilicic acid, 0.28% formaldehyde and 50 g/L Na2CO3. Sections were then washed again in 0.5% acetic acid, incubated 5 min in 1% gold chloride before rinsing in distilled water. Fixation of the staining was then performed by washing sections 3 times in 1% sodium thiosulfate, after which sections were dehydrated in increasing ethanol concentrations and xylene before mounting using Eukitt (Dutscher, France).

2.3. Image analysis

Images of AT8/Iba1/DAPI, pSer422/GFAP immunostainings and

Gallyas were acquired at 20× using the slide scanner Axio ScanZ.1 (Carl Zeiss, Jena, Germany). Image files were then converted into TIFF format and reduced to 50% of full resolution size. Manual segmentation of the CA1 region was performed on 3 sections of the hippocampus at 1.7, 2.3 and 2.9 mm posterior from bregma. For AT8, Iba1, pSer422 and GFAP, the fluorescence levels were quantified with ImageJ, and Gallyas positive neurons were counted on those 3 sections. As a surrogate index of neuronal degeneration, the thickness of the pyramidal neuronal CA1 layer was assessed on the DAPI staining on three different areas and pooled for each section. The analysis of the AT100 labelling was performed with Mercator (ExploraNovaTM) by counting the number of AT100 positive neurons on 3 sections of the hippocampus at 1.7, 2.3, 2.9 mm posterior from bregma. All quantifications were performed blindly.

2.4. Real-time quantitative PCR

After euthanasia with a lethal dose of pentobarbital, animals were perfused by 30 mL sterile PBS to wash the brain from blood, then the hippocampus were dissected on ice and frozen in liquid nitrogen before storage at −80 °C. Frozen hippocampus structures were lysed in 1 mL of TRIzol using Precellys homogenizer (OzymeTM). 200 μL of chloroform (Merck) were added in each tube before centrifugation at 12000*g* for 15 min at 6 °C. Aqueous phase was separated and total RNA was precipitated by adding 250 μL isopropanol (VWR) and washed two times with 500 μL 75% ethanol (VWR). Then, RNA was resuspended in 20 μL of RNase-free H2O (Gibco) and RNA concentration was measured on a Nanodrop (Spectrophotometer ND-100, Labtech). The samples were stored at −80 °C before transcriptomic analysis. *Ppia* and *Gapdh* were used as reference genes pair for quantification. Primers sequence are described in Supplementary Table 2.

2.5. Behavioral studies

Circadian activity: mice were monitored for 23 h using a video camera and automatic tracking of the Ethovision™ software in Phenotyper™ chambers (Noldus Information Technology Inc). Food and drinking water were available ad libitum. Moving distance was quantified for each hour of the recording session in order to evaluate motor behavior and circadian rhythm.

Elevated Plus Maze: the maze was set at a height of 50 cm and consisted of four Plexiglas arms. Two of the arms have 15 cm high walls (closed arms), while the others two are open. Individual mice were placed in the middle section of the apparatus facing an open arm, and left to explore the maze for 6 min. Time spent in open and closed arms was measured by a video camera connected to a computer and analyzed with Ethovision™ video-tracking system and frequency of head-dipping into open arms was analyzed by manual tracking.

Novel Object Recognition (NOR) test: memory was first evaluated using an object recognition test in a V-maze (Puighermanal et al., 2009). For this, a discrimination index, between −1 and 1, is calculated in order to evaluate an exploration preference for a new object (index 1) with respect to an already known object (index −1). The test is performed in a V-shaped chamber to reduce the variability associated with the experimenter. The device consists of two black Plexiglas arms and is illuminated at 50 lx at the end of each arm. For each phase, the distance traveled was measured by video-camera and analyzed with the EthoVision™ video-tracking system and the time spent exploring each object was measured manually. During the first habituation phase, each mouse was placed at the angle of the V, and left in the maze without object for a 9 min training session. The next day, two identical objects (cylinders) were placed at the end of each arm in the same place, and the time spent by the mouse exploring each object was recorded for a session lasting 9 min. The third day one of the cylinder was replaced by a new object (i.e. a Lego™) and the test phase was recorded for 6 min. The discrimination index was calculated with the following formula: (time spent exploring new object - time to explore old object) / total time of exploration.

Morris Water Maze (MWM) test: the maze consisted in a large circular tank filled with an opaque mix of water and white painting kept between 20 °C and 22 °C. An escape platform was submerged 0.5 cm under the water level. Visual clues were provided by different geometrical forms placed on the four surrounding walls. On day first mice were trained to find the platform on 4 trials at 20–30 min interval, location of the platform and starting point of the mice being changed for each trial. Escape latency was defined as the time required for the mouse to reach the platform and to stay there for at least 3 s. During the subsequent learning phase, location of the platform remained the same and mice performed 3 trials every day for 5 days. Starting point was changed for each trial. If a mouse did not find the platform after 1 min the experimenter guides it to the platform and let it rest there for 30 s. Escape latency was recorded for each trial. Probe test was performed 72 h after the last training day in order to assess long term memory. During this phase, platform was removed and mice were let freely swimming in the pool for 1 min. The pool was divided in four virtual quadrants: the target quadrant (TQ) in which the platform was located, the quadrant opposite to the TQ (OQ), and the two quadrants adjacent to the TQ (AQ). Time spent in virtual quadrants and total distance to the platform previous location were measured.

2.6. Statistical analysis

Results are presented as mean ± standard error of the mean (SEM). Statistical analysis were carried out using Statistica 13 software (Statsoft, Tulsa, OK, USA), except for Sholl analysis and pSer422 and GFAP immunolabeling quantification which were processed with Prism 8 (GraphPad Software, San Diego, CA, USA). Data were assessed for normality and homogeneity of variance by the Levene test prior to analysis. Unless otherwise mentioned, data fulfilling the criteria were analyzed by two-way ANOVA followed by Bonferroni's post hoc tests for pairwise comparisons. A non-parametric equivalent was used if normality and homogeneity of variance was not reached. Annotations used to indicate level of significance were as follows: $*P < 0.05$, $**P < 0.01$, $***P < 0.001$. To determine frequency distribution of the Ramification Index after Sholl analysis of microglia or astrocytes, a number of bins to classify the cells was established following the log2 of sample size at the three studied ages, and the smallest value among the three timepoints was selected for subsequent analysis. Statistical significance of distribution into bins was then assessed by X^2 test. Results of the Phenotyper™ were analyzed by ANOVA repeated-measures, after confirmation of normality and homogeneity of variance by the Levene test as well as sphericity by the Mauchley test. Results of the Elevated Plus Maze test were analyzed by Student's *t*-test after assessment of normality and homogeneity of variance by the Levene test. NOR test was analyzed by Student's *t*-test comparing the discrimination index to a value of 0. Learning phase of the MWM test was analyzed by ANOVA repeated-measures, after assessment of normality and homogeneity of variance by the Levene test as well as the sphericity by the Mauchley test. Results of the probe test were analyzed by Student's *t*-test comparing the percentage of time spent in each quadrant to a value of 25%.

3. Results

3.1. Trem2 deficiency leads to an increase of hyperphosphorylation and aggregation of Tau at 12 months in the THY-Tau22 mouse model

To investigate the role of TREM2 signaling on the progression of tauopathy, we crossed *Trem2*$^{-/-}$ mice (Turnbull et al., 2006) and wild-type littermates with THY-Tau22 heterozygous transgenic mice (Schindowski et al., 2006) to generate four different genotypes: THY-Tau22$^{Tg/-}$:*Trem2*$^{+/+}$, THY-Tau22$^{Tg/-}$:*Trem2*$^{-/-}$, THY-Tau22$^{-/-}$:*Trem2*$^{+/+}$, THY-Tau22$^{-/-}$:*Trem2*$^{-/-}$, referred below as Tau22, Tau22:*Trem2*$^{-/-}$, wild-type and *Trem2*$^{-/-}$ respectively. We first evaluated in

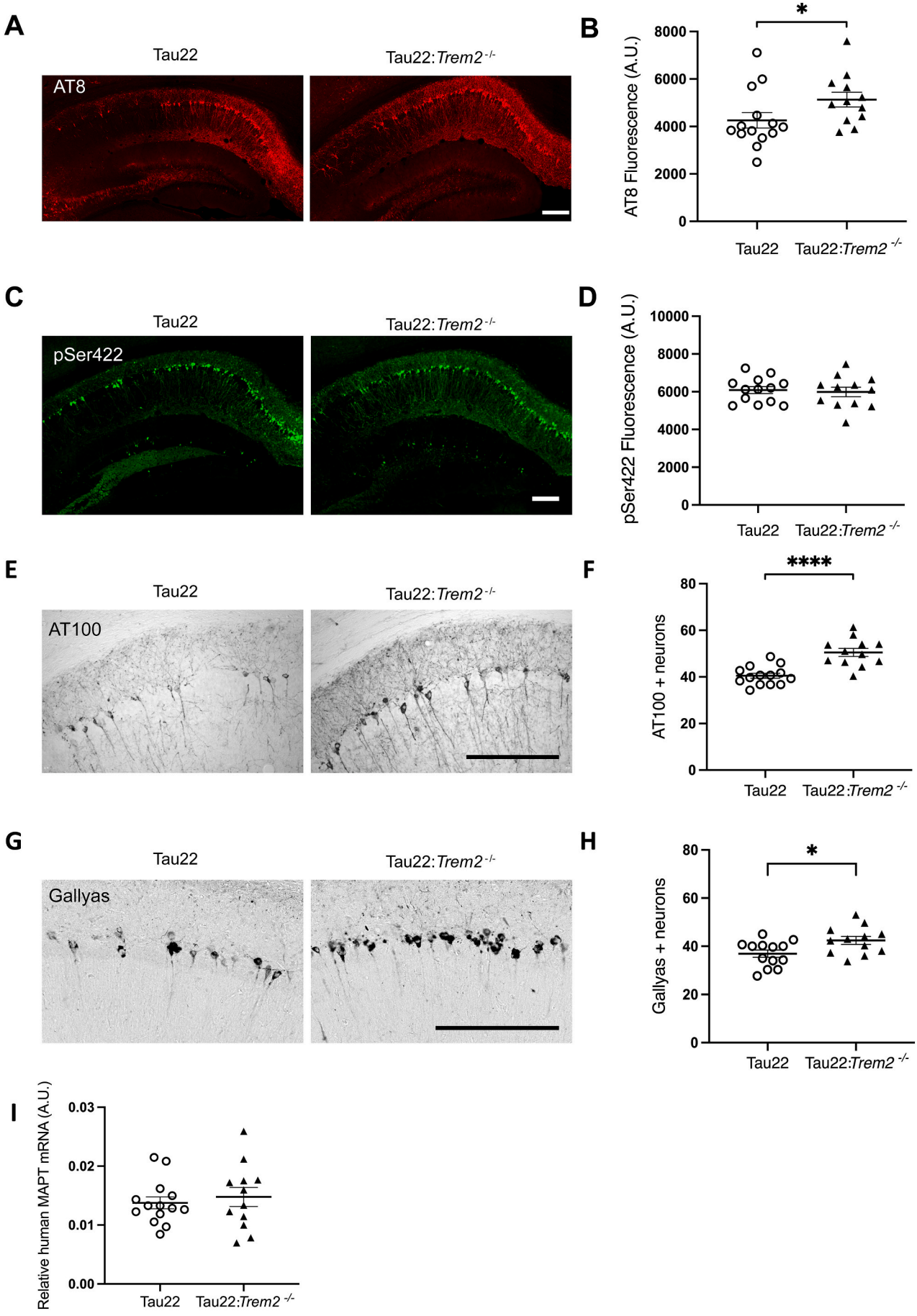

(caption on next page)

Fig. 1. TREM2 deficiency led to an increase in Tau phosphorylation and aggregation at 12 months in Tau22 mice. Immunofluorescence labelling of the CA1 layer of the hippocampus using the human phospho-Tau specific epitopes AT8 (A) and pSer422 (C). Fluorescent signal intensity of the whole CA1 layer was quantified using ImageJ (B, D). Tau misconformation was revealed by AT100 immunohistochemical staining (E) and positive neurons were manually counted in each group (F). Mature aggregates were detected using Gallyas staining (G) and manually counted in each group (H). Consistency of THY-Tau22 trangene expression among groups was assessed by RT-QPCR on the human MAPT gene on hippocampal samples, and showed that *Trem2* genotype did not modify transgene expression (I). Results were normalized by expression of the housekeeping genes *Gapdh* and *Ppia*. Data represents mean ± SEM, n = 14 for Tau 22 and n = 12 for Tau22:*Trem2*$^{-/-}$, these data are presented stratified by sex on Fig. S2. Scale bar: 200 μm.

CA1 layer of the hippocampus Tau hyperphosphorylation by immunofluorescence using antibodies raised against pSer202/pThr205 (AT8), pSer422, and Tau misconformation by immunohistochemistry using AT100, an antibody detecting a late-stage phospho-epitope mostly found on intracellular NFTs in human (Allen et al., 2002; Augustinack et al., 2002). Quantification of fluorescence levels for markers of hyperphosphorylation or AT100+ cells counting did not reveal any significant difference between Tau22 and Tau22:*Trem2*$^{-/-}$ at 3 months (Mann-Whitney test, $p = 0.91$ for AT8, Fig. S1A—B; Student's *t*-test, $p = 0.30$ for pSer422, Fig. S1C–D; Student's *t*-test, $p = 0.44$ for AT100, Fig. S1E–F) and 6 months of age (Student's *t*-test, $p = 0.19$ for AT8, Fig. S1A–B; $p = 0.74$ for pSer422, Fig. S1C–D; $p = 0.70$ for AT100, Fig. S1E–F). Interestingly, TREM2 deficiency led to a significant increase of tauopathy at a later pathological stage. At 12 months, Tau22:*Trem2*$^{-/-}$ mice indeed showed more AT8 labelling (multifactorial ANOVA, $F = 4.5$, $p = 0.045$, Fig. 1A-B), as well as higher number of AT100-positive (multifactorial ANOVA, $F = 24.43$, $p < 0.001$, Fig. 1E-F) and Gallyas-positive neurons (multifactorial ANOVA, $F = 5.841$, $p = 0.025$, Fig. 1G-H) as compared to littermate Tau22 mice. Such worsening of tauopathy due to TREM2 deficiency was similar in males and females (Fig. S2). To exclude the possibility that exacerbated tauopathy in a TREM2-deficient context resulted from an increase in transgene expression, we used RT-QPCR to quantify human MAPT expression. No difference was observed between Tau22 and Tau22:*Trem2*$^{-/-}$ animals at any studied age (Figs. 1I and S1G—H).

3.2. Tauopathy worsening in Trem2-deficient Tau22 mice is associated with microglial sub-activation

Given the previous data obtained in THY-Tau22 model and associating microglial activation to Tau pathology development (Ising, 2019; Laurent et al., 2017), we next examined whether TREM2 deficiency led to a change in the neuroinflammatory response generated by tauopathy. To assess the microglia response, we quantified the intensity of Iba1immunolabeling as an index of activation state, and we counted the number of microglial cells using the nuclear marker PU.1, a monocyte-specific transcription factor expressed in myeloid cells and lymphoid B cells (Mak et al., 2011). There was no difference in the overall level of Iba1 immunofluorescence in the CA1 layer between the 4 genotypes at 3 months (multifactorial ANOVA, $F = 2.41$, $p = 0.13$ for the *Trem2* genotype, $F = 0.019$, $p = 0.89$ for Tau22, Fig. S3A—B), 6 months (multifactorial ANOVA $F = 1.42$, $p = 0.24$ for *Trem2* genotype and $F = 0.53$, $p = 0.47$ for Tau22, Fig. S3C—D) or 12 months (Kruskal-Wallis ANOVA, $p = 0.13$, Fig. 2A-B). Moreover, all genotypes exhibited the same number of PU.1 positive nuclei at 6 or 12 months (Figs. S3F-G and 2C—D). To further characterize the microglial activation state, we also performed a Sholl analysis (Fig. 2E-J). Analysis of the microglial ramification index in Tau22 animals indicated that the cells adopted a more amoeboid morphology with age, a phenomenon which was significantly attenuated in TREM2-deficient animals (Fig. 2G). The classification of cells according to the ramification index particularly revealed a significantly smaller ramification index in Tau22 mice compared to Tau22:*Trem2*$^{-/-}$ at 12 months of age (Fig. 2H-J). We also observed an increase in the ramification index with age in wild-type and *Trem2*$^{-/-}$ animals, but no effect of TREM2 deficiency in this context (Fig. S3I-L). Overall, these data suggest a close association between the reduced microgliosis observed in TREM2-deficient Tau22 animals and the worsening of tauopathy observed in aged animals.

Finally, we also used RT-QPCR to evaluate the expression of a set of genes involved in neuroinflammatory processes (Figs. 3, S4 and S5). Regardless of their *Trem2* genotype, 3 months-old Tau22 mice expressed higher levels of *Gfap* (multifactorial ANOVA, $F = 21.35$, $p < 0.001$) and *Serpina3n* (multifactorial ANOVA, $F = 18.13$, $p < 0.001$) compared to WT, two markers of reactive astrocytes, as well as *Tmem119* (multifactorial ANOVA, $F = 6.31$, $p = 0.017$) and *Aif1* (Kruskal-Wallis ANOVA by multiple comparison, $p = 0.046$), two microglial markers. At this age, only *Dap12* (multifactorial ANOVA, $F = 11.71$,$p = 0.0018$) and the pro-inflammatory cytokine *Tnfα* (multifactorial ANOVA, $F = 5.75$, $p = 0.041$) were significantly down-regulated in Tau22:*Trem2*$^{-/-}$ animals compared to Tau22 (Fig. S4). At 6 months (Fig. S5), only *Gfap* (multifactorial ANOVA, $F = 7.08$, $p = 0.016$) and *Tnfα* (multifactorial ANOVA, $F = 4.751$, $p = 0.0421$) were significantly upregulated in Tau22 mice, whether they express *Trem2* or not. Consistent with our histological results, most of the microglial markers were up-regulated in 12 month-old Tau22 animals compared to wild-type (Fig. 3). Interestingly, the markers of microglial activation toward a less homeostatic state (*CD68*, *Dap12*, *Aif1*, *Il-1b*, *Tgfβ*, *Tmem119*) were significantly down-regulated in Tau22:*Trem2*$^{-/-}$ animals compared to Tau22. Of note at that age, a sex-dependent effect was observed for some genes, whose differential expression was more accentuated in males: *Cd68* (multifactorial ANOVA, $F = 9.16$, Bonferroni post-hoc test, $p = 0.0006$), *Aif1* (Kruskal-Wallis ANOVA by multiple comparison, $p = 0.027$), *Tgf-β* (multifactorial ANOVA, $F = 6.56$; Bonferroni hoc, $p = 0.0047$) and *Gfap* (Kruskal-Wallis ANOVA by multiple comparison, $p = 0.0034$) were significantly up-regulated only in Tau22 males compared to wild-type.

Recent evidences suggest that activated microglia can regulate astrocytes reactivity (Liddelow et al., 2017). Hence, we tested the hypothesis that reduced microglial activation in TREM2 deficient mice could impact astrogliosis. We quantified the expression level of GFAP on immunostained sections (Figs. 4 and S6). In agreement with the literature (Laurent et al., 2016; Laurent et al., 2017; Schindowski et al., 2006), expression of the Tau transgene induced a strong astrogliosis throughout the hippocampus and in particular in the CA1 layer (multifactorial ANOVA, $F = 21.075$, $p < 0.001$). However, TREM2 deficiency did not influence astroglial activation (Fig. 4A-B). To catch potential subtle changes in astrocyte morphology indicative of astrocyte reactivity, we also performed a Sholl analysis of these cells and did not uncover change in complexity in Tau22:*Trem2*$^{-/-}$ animals at any time-points tested (Fig. 4C-G).

3.3. TREM2-deficiency has a limited impact on hippocampal morphology in THY-Tau22 mice

We next assessed whether TREM2 deficiency was associated with a faster degeneration of CA1 pyramidal neurons which strongly develop Tau pathology in this mouse model. To that aim, we quantified the area of CA1 and the thickness of the pyramidal neurons nuclei layer as surrogate markers of hippocampal atrophy. Already at three months, we observed a thinner CA1 pyramidal nuclei layer in Tau22 animals independently of *Trem2* genotype (multifactorial ANOVA, $F = 14.36$, $p < 0.001$, Fig. 5A-B), reaching 17% decrease at 12 months of age (Mann Whitney, $p < 0.001$, Fig. 5E-F). The six months' time-point showed the same tendency, although not significantly due to small sample size and greater heterogeneity (Kruskal-Wallis ANOVA by multiple comparison, $p = 0.19$, Fig. 5C-D). This result was corroborated by quantification of the whole CA1 layer area, that was significantly reduced in Tau22 mice

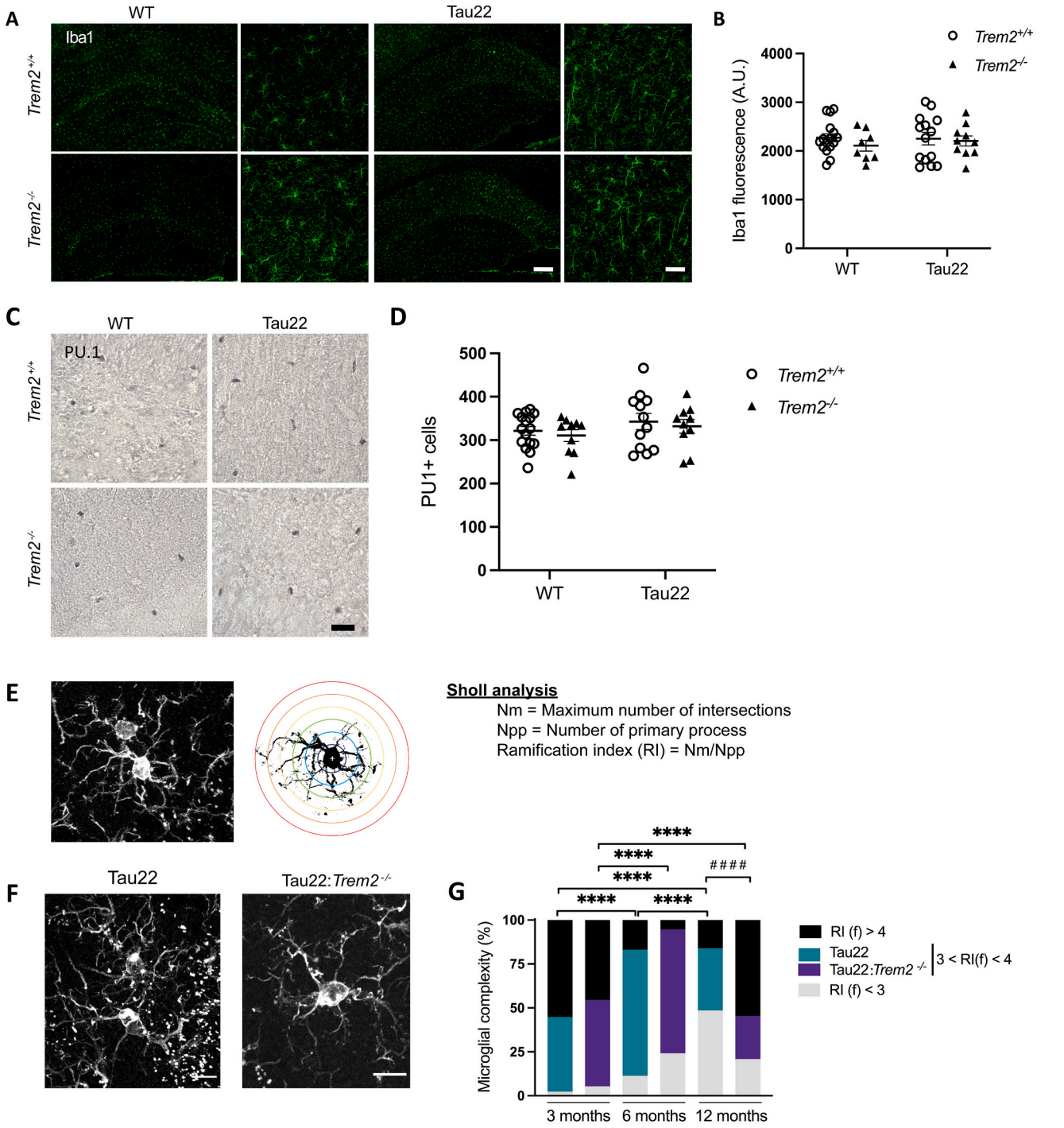

(caption on next page)

Fig. 2. Morphological characterization of microglia in 12 month-old mice showed a reduced microglial activation in Tau22:*Trem2*$^{-/-}$ animals. (A) Representative micrographs of Iba1 immunofluorescence and (B) quantification of the signal of wild-type, *Trem2*$^{-/-}$, Tau22 and Tau22:*Trem2*$^{-/-}$ animals. (C) Representative micrographs of PU.1 immunohistochemical staining and (D) PU.1 positive nuclei counts in wild-type, *Trem2*$^{-/-}$, Tau22 and Tau22:*Trem2*$^{-/-}$ animals. (E) Representative confocal image of an Iba1 stained microglia (left) and corresponding binarization (right) for Sholl analysis. The formula for calculating the ramification index is summarized on the right. (F) Representative confocal images of Tau22 and Tau22:*Trem2*$^{-/-}$ microglia. (G-J) Sholl analysis of microglial morphology in the CA1 layer based on Iba1 staining for Tau22 and Tau:*Trem2*$^{-/-}$ animals at 3-, 6- and 12 months of age. A significant decrease in the morphology of microglial complexity is observed with age in both groups although to a lesser extent in Tau22:*Trem2*$^{-/-}$ animals. Consequently microglia have a significantly less amoeboid phenotype in Tau22:*Trem2*$^{-/-}$ mice compared to Tau22 at 12 months of age. Scale bars: 200 μm in A (left), 50 μm in A (right) and C, 10 μm in E and F. Data in B and D represents mean ± SEM, n = 6 M + 10F for WT, n = 6 M + 4F for *Trem2*$^{-/-}$, n = 7 M + 7F for Tau22 and n = 5 M + 7F for Tau22:*Trem2*$^{-/-}$ (M: male, F: female).

compared to wild-type at six (multifactorial ANOVA, F = 8.07, p = 0.0086, Fig. 5H) and twelve months (multifactorial ANOVA, F = 7.85, p = 0.0075, Fig. 5I) regardless of *Trem2* genotype. Interestingly, this quantification revealed a slightly higher CA1 area in Tau22:*Trem2*$^{-/-}$ animals compared to Tau22 at 6- (13% increase) and 12 (10% increase) months of age (Fig. 5H-I). These results show that TREM2 deficiency mitigates CA1 atrophy induced by Tau pathology.

3.4. The poor performances of Tau22 mice in cognitive tests is not restored by Trem2 deficiency

To investigate whether differences in tauopathy, neuroinflammation and neurodegeneration observed in Tau22:*Trem2*$^{-/-}$ mice compared to Tau22 led to behavioral changes, we carried out a battery of cognitive tests on these animals at the age of 10 months, as well as on wild-type and *Trem2*$^{-/-}$ littermate controls. These two control groups performed equally well in all the tests, therefore showing that TREM2 deficiency in itself had no effect on mice performance (Fig. 6). Conversely, and as expected, THY-Tau22 mice exhibited important behavioral dysfunction (Fig. 6). The Phenotyper™ did not reveal any significant difference in the basal activity between Tau22 and Tau22:*Trem2*$^{-/-}$ mice (ANOVA repeated-measures, F = 1.29, p = 0.27, Fig. 6A), indicating that TREM2 deficiency does not seem to impact the overall mice activity. However, it should be noted that TREM2 deficient mice showed a trend toward increased activity at the beginning of the dark phase (i.e. between 11 h and 17 h) and of the light phase (i.e. between 22 h and 23 h), and conversely a trend toward decreased activity at the end of the dark phase (i.e. between 18 h and 21 h), without these differences reaching statistical threshold. In the elevated plus maze, Tau22:*Trem2*$^{-/-}$ mice showed a tendency to spend more time in the open arms (Student's t-test, p = 0.063; Fig. 6C). In addition, Tau22:*Trem2*$^{-/-}$ mice spent significantly more time leaning at the edges of the maze (Student's t-test, p = 0.0061; Fig. 6D). It should also be noted that all mice have spent ~50% of the time in the open arms, thereby demonstrating a low level of general anxiety of Tau22 mice compared to wild-type mice (Figs. 6C-D and S7C—D). In the NOR test, we did not detect any difference between Tau22 and Tau22:*Trem2*$^{-/-}$ mice (Student's t-test, p = 0.81; Fig. 6B). In addition, none of the groups explored the novel object significantly more than the familiar one (Student's t-test with respect to 0, p = 0.12 for Tau22 mice, p = 0,26 for Tau22:*Trem2*$^{-/-}$). Tau22 mice therefore presented a memory defect at 10 months related to object recognition, which was not rescued by TREM2 deficiency. In the MWM test, the latency to find the platform significantly decreased over days for both groups (ANOVA repeated-measures, p < 0.001; Fig. 6E). Furthermore, no difference in learning was observed between Tau22 and Tau22:*Trem2*$^{-/-}$ mice, showing that TREM2 deficiency has no further effect on the learning ability in 10-month-old Tau22 mice (ANOVA repeated-measures, p = 0.65; Fig. 6E). We next assessed long-term memory using a retention test performed 72 h after the last training day. None of the group showed a preference for the target quadrant (Student's t-test relative to 25%, p = 0.11 for Tau22 mice, p = 0.26% for Tau22:*Trem2*$^{-/-}$ mice; Fig. 6F), showing an overall long-term memory deficit for Tau22 mice, which was not impacted by TREM2 expression. Overall, this behavioral study showed that THY-Tau22 mice had important memory deficits at 10 months, which were neither worsened nor rescued by TREM2 deficiency.

4. Discussion

Deciphering the role of microglia in the progression of tauopathy is an important issue for understanding the etiology of AD and the search for new therapeutic avenues for this pathology. In this context, the TREM2 microglial receptor is of particular importance because some of its polymorphisms increase the risk of developing the disease (Guerreiro et al., 2013; Jonsson et al., 2013), and TREM2 signaling has been shown to lead to the appearance of a subpopulation of microglial cells characteristic of neurodegenerative diseases (Keren-Shaul et al., 2017). Several studies have reported the potential of TREM2 in mouse models of tauopathy, with partially contradictory results. Here, we investigated the effect of invalidation of *Trem2* on THY-Tau22 mice, a well-characterized model of tauopathy. We observed an increased Tau hyperphosphorylation and a greater number of neurons containing aggregated forms, only in the advanced stages of the pathology. This increase in tauopathy lesions was associated to a slight but significant decrease in microglial activation.

Based on the hypothesis that less neuroinflammation in *Trem2*$^{-/-}$ mice would allow a better functioning of remaining neurons that are not affected by tauopathy, we carried out a behavioral study on 10 month-old animals. TREM2 deficiency having a slightly neuroprotective effect resulting in a preservation of the volume of the CA1 layer at this age (Fig. 5I), we expected to observe better cognitive performances in Tau22:*Trem2*$^{-/-}$ mice. The NOR and the MWM tests however showed that *Trem2* invalidation had no effect on THY-Tau22 mice memory deficits at this age (Fig. 6). This suggests that in the THY-Tau22 model, reducing microgliosis does not lead to improve function of neurons that remain functional at 10 months of age and could be impaired by microglia-mediated neuroinflammation. Importantly, we carried out these experiments at an age at which the deficits of the mice are maximum (Schindowski et al., 2006; Van der Jeugd et al., 2013b). Therefore, it remains possible that the increase Tau pathology seen in *Trem2*-deleted Tau22 mice, which is fairly correlated to memory deficits in this model (Van der Jeugd et al., 2013b), cannot translate at late stage with further detrimental effects on memory abilities. This would require additional behavioral analysis at an earlier time, i.e. when the deficits of THY-Tau22 mice are still subtle. Importantly, we show here that *Trem2*$^{-/-}$ mice are not different from wild-type mice in all the behavioral tests we have studied (Fig. 6), thus ensuring that invalidation of this gene in itself does not induce any bias that would complicate the interpretation of these experiments.

The effect of TREM2 deficiency has already been studied in several transgenic models of pure tauopathy. The first studies published by Jiang et al. suggest that activation of the TREM2 signaling pathway in the PS19 transgenic line reduces neurodegeneration and hyperphosphorylation of Tau (Jiang et al., 2014; Jiang et al., 2015). However, it is difficult to compare these results with our study, because in the case of the work of Jiang et al., the modulation of TREM2 signaling pathway was based on lentiviral gene transfer to overexpress or silence *Trem2* expression in vivo. In addition, these studies did not provide definitive proof of efficient microglial targeting by gene transfer. Other studies used a methodology similar to ours, based on crossing tauopathic mice with *Trem2* knockout mice, but with different models of tauopathy. Leyns et al. showed that TREM2 deficiency leads to a decrease in neurodegeneration and neuroinflammation in PS19 mice (Leyns et al.,

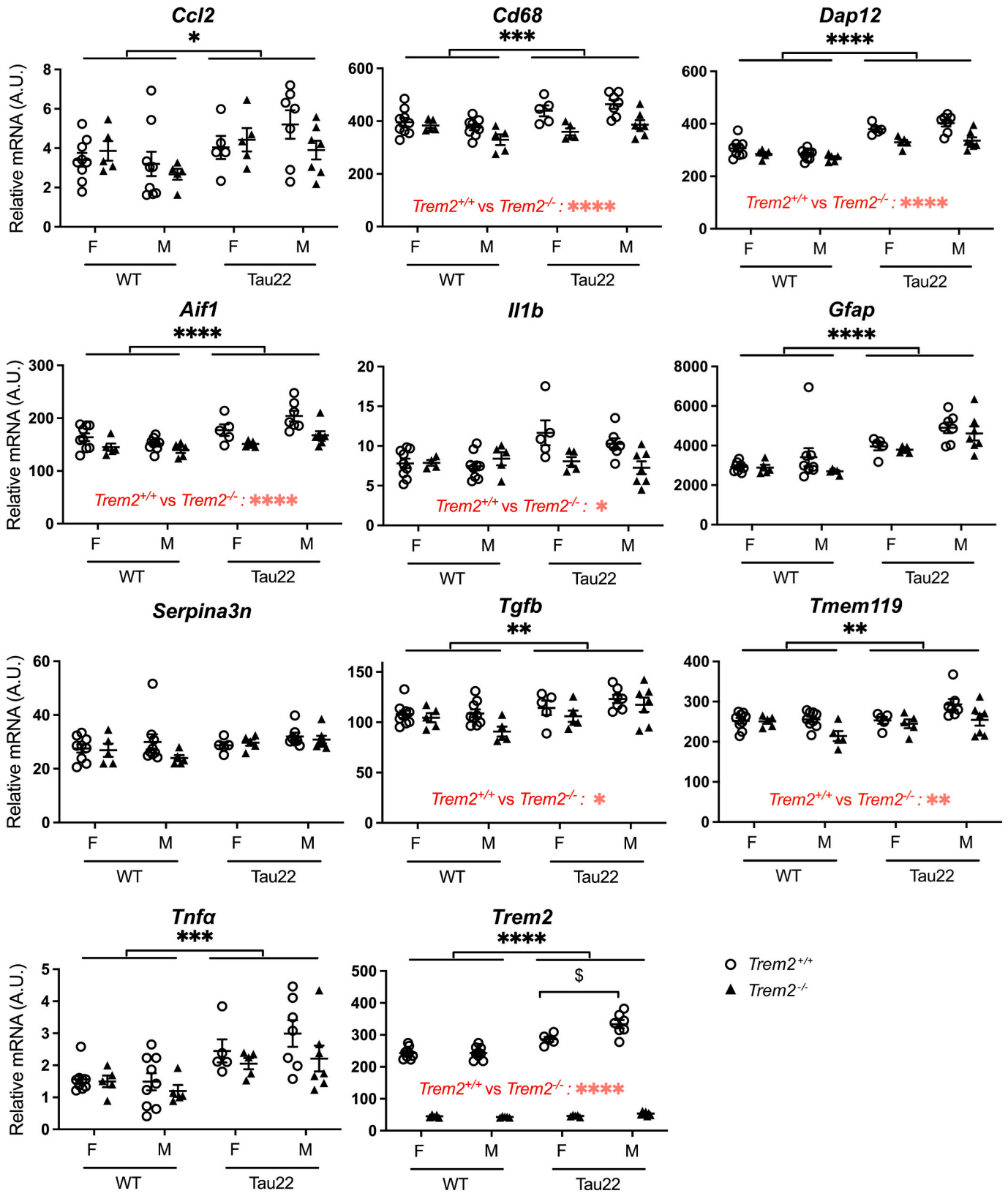

Fig. 3. Level of expression of neuroinflammatory genes quantified by RT-QPCR at twelve months of age. mRNA were extracted from total hippocampus. Results were normalized using *Gapdh* and *Ppia* housekeeping genes expression. Statistical data reported in black refers to the effect of THY-Tau22 transgene expression, and in red refers to differences between *Trem2*$^{+/+}$ and *Trem2*$^{-/-}$ mice, independently of the THY-Tau22 genotype. Data are presented as mean ± SEM, n = 9 M + 9F for WT, n = 5 M + 5F for *Trem2*$^{-/-}$, n = 7 M + 7F for Tau22, and n = 7 M + 5F for Tau22:*Trem2*$^{-/-}$ (M: male, F: female). $: $p = 0.0011$ (M vs F). (For interpretation of the references to colour in this figure legend, the reader is referred to the web version of this article.)

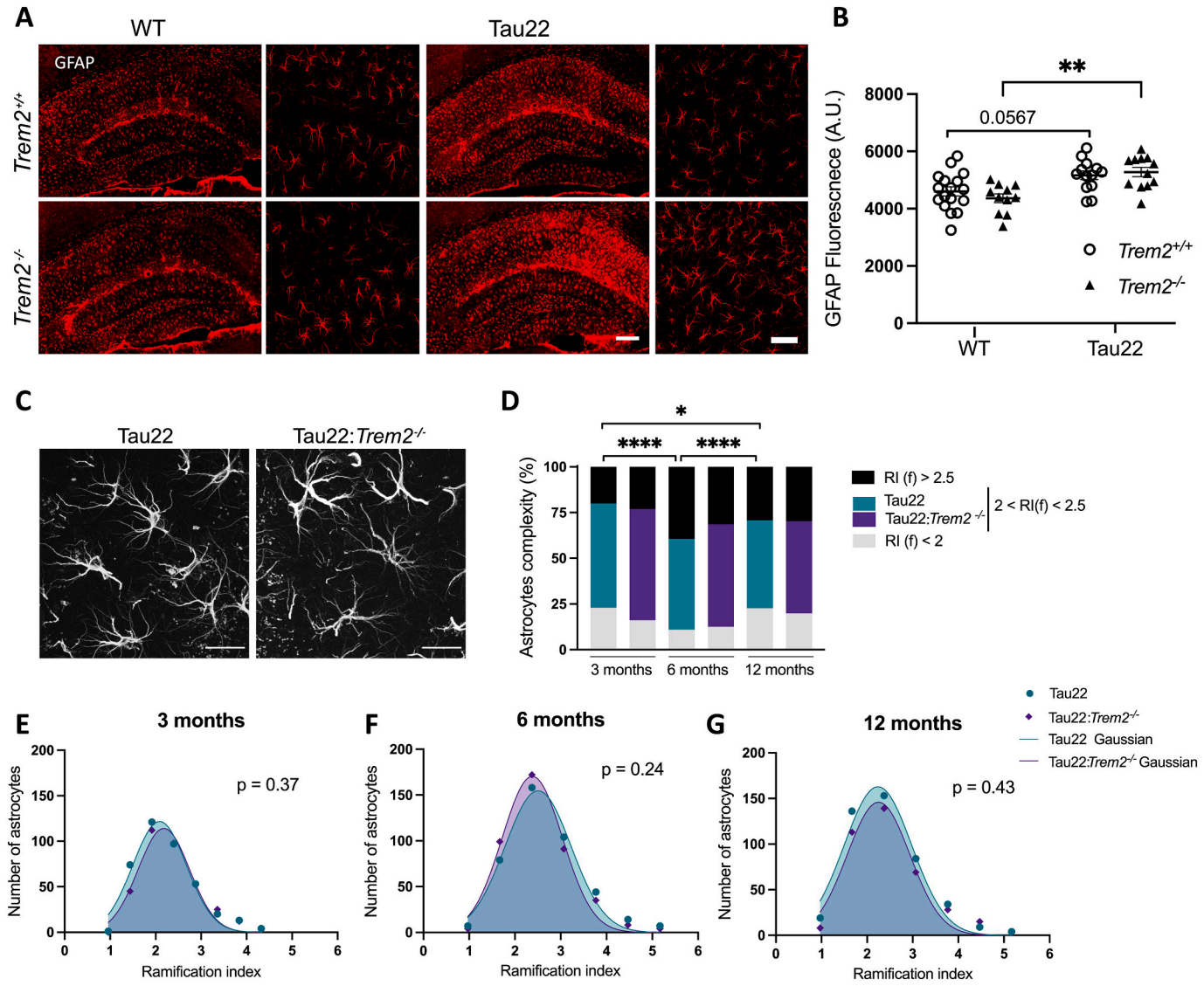

Fig. 4. The strong astrogliosis occuring in Tau22 mice was not affected by TREM2 deficiency. (A) GFAP immunofluorescence showing the strong astrogliosis induced by expression of the THY-Tau22 transgene in the CA1 layer of 12 months-old animals. (B) Quantification of GFAP immunofluorescence in CA1 layer. (C) Representative confocal images of GFAP immunofluorescence used for Sholl analysis of astrocytes morphology. (D-G) Sholl analysis of astrocytic morphology in the CA1 layer based on GFAP staining for Tau22 and Tau22:*Trem2*$^{-/-}$ animals at 3-, 6- and 12 months of age. Repartition of the ramification index (RI) is similar in the two groups at 3-, 6- and 12 months of age (*E*-G), indicating that astrogliosis is similar between Tau22 and Tau22:*Trem2*$^{-/-}$ animals. Scale bar: 200 μm in A (left), 50 μm in A (right), 20 μm in C. Data in B are presented as mean ± SEM, n = 7 M + 10F for WT, n = 6 M + 5F for *Trem2*$^{-/-}$, n = 7 M + 7F for Tau22, and n = 7 M + 5F for Tau22:*Trem2*$^{-/-}$ (M: male, F: female).

2017). This is in line with our results showing that TREM2 is involved in the microglial activation in response to tauopathy, this effect is however less marked in our study most certainly because the microglial activation is stronger in the PS19 model than in the THY-Tau22 model, and occurs even before the appearance of lesions characteristic of tauopathy (Yoshiyama et al., 2007). In sharp contrast, Leyns et al. did not observe changes in the course of tauopathy, while our data report a significant enhancement. A second study also based on the PS19 line reports similar results on the course of tauopathy in animals deficient in TREM2 (*Trem2*$^{-/-}$), but surprisingly an increase in tauopathy in haplo-insufficient animals (*Trem2*$^{+/-}$) (Sayed et al., 2018). Bemiller et al. used the hTau mouse line which expresses all the wild-type human isoforms of Tau in a knockout context for the mouse *Mapt* gene (Andorfer et al., 2003). In this model, TREM2 deficiency also led to a reduction in microgliosis, but also to an increase in hyper-phosphorylation and aggregation of Tau in the cortex (Bemiller et al., 2017), contrarily to what was observed in the PS19 transgenic line. This is in line with our own results and strongly suggests that a decrease in microglial activation induces an increase in tauopathy lesions which can be explained in several ways. The absence of microglial activation may lead to an acceleration of tauopathy in neurons by a modification of the crosstalk between these two cell types, which is known to take place by multiple signaling pathways such as neurotransmitters, cytokines, or purinergic receptors (De Schepper, 2020). Alternatively, it is possible that the decrease in microglial activation slows the clearance of damaged and dysfunctional Tau-bearing neurons. The fact that we observe a slight increase in the surface area of CA1 in the present study (Fig. 5G-I) and a decrease in the expression of markers of microglial activation (Fig. 3) is rather in favor of this last hypothesis which is further reinforced by the fact that the microglia are able to phagocytose pathological species of the Tau protein (Hopp et al., 2018). A strong astrogliosis occurs in THY-Tau22 mice, as we have shown here (Figs. 4 and S6) and previously (Laurent et al., 2017; Schindowski et al., 2006). This astrogliosis was unchanged in Tau22:*Trem2*$^{-/-}$ mice suggesting

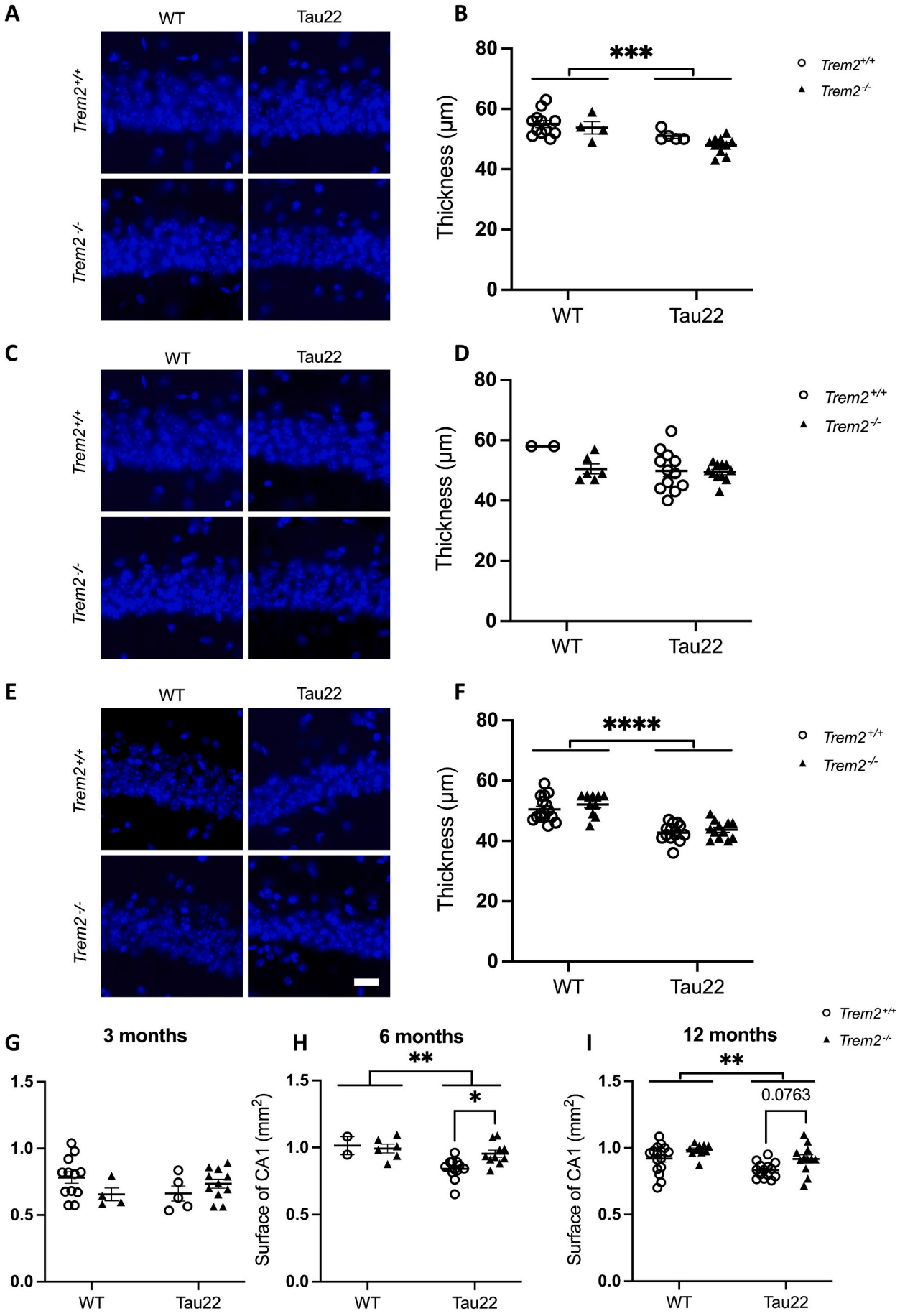

(caption on next page)

Fig. 5. Assessment of neuronal degeneration in the CA1 layer of the hippocampus at 3, 6 and 12 months. Representative epifluorescence micrographs showing DAPI-stained nuclei in wild-type, *Trem2*$^{-/-}$, Tau22 and Tau22:*Trem2*$^{-/-}$ animals at 3- (A), 6- (C) and 12 months. (E). Quantification of pyramidal nuclei layer thickness at 3- (B), 6- (D) and 12 months (F) showed a significant cell loss in THY-Tau22 expressing mice and no effect of TREM2 deficiency. Atrophy was estimated by quantification of CA1 area on coronal sections (G-I). In accordance with measurement of pyramidal neuronal nuclei layer thickness, a significant atrophy was detected in Tau22 mice at 6- (H) and 12 months (I). At both time-points, CA1 area was partially protected from shrinkage in TREM2 deficient mice (H–I, $p = 0.0763$ at 12 months). Data represents mean ± SEM. Scale bar: 20 µm. n = 12, 2 and 17 for WT, $n = 4$, 6 and 10 for *Trem2*$^{-/-}$, n = 5, 12 and 14 for Tau22, and $n = 11$, 10 and 12 Tau22:*Trem2*$^{-/-}$, at 3, 6 and 12 months respectively. All the groups were composed of about 50%M and 50%F, except WT at 6 months (2 M), *Trem2*$^{-/-}$ at 3- (1 M + 3F) and 6-months (6F), and Tau22: *Trem2*$^{-/-}$ at 6 months (7 M + 3F), (M: male, F: female).

that microglial homeostatic state has no effect on astrocyte activation in THY-Tau22 mice, excluding a role of the TREM2 signaling pathway in this context.

Initially, the role of TREM2 in AD was studied in animal models of amyloidosis (Jay et al., 2017; Jay et al., 2015; Parhizkar et al., 2019; Wang et al., 2015; Wang et al., 2016; Yuan et al., 2016), because it has long been known that reactive microglia are found in the immediate vicinity of senile plaques. Although the first published studies initially seemed to report conflicting results, there now seems to be a consensus that TREM2 engagement contributes to the maintenance of microglial metabolism in an active state that allows these cells to contain the progression of the amyloid load by compacting senile plaques (Ulland et al., 2017; Wang et al., 2016). Very interestingly, a recent publication reports the effect of TREM2 deficiency in a model exhibiting both ß-

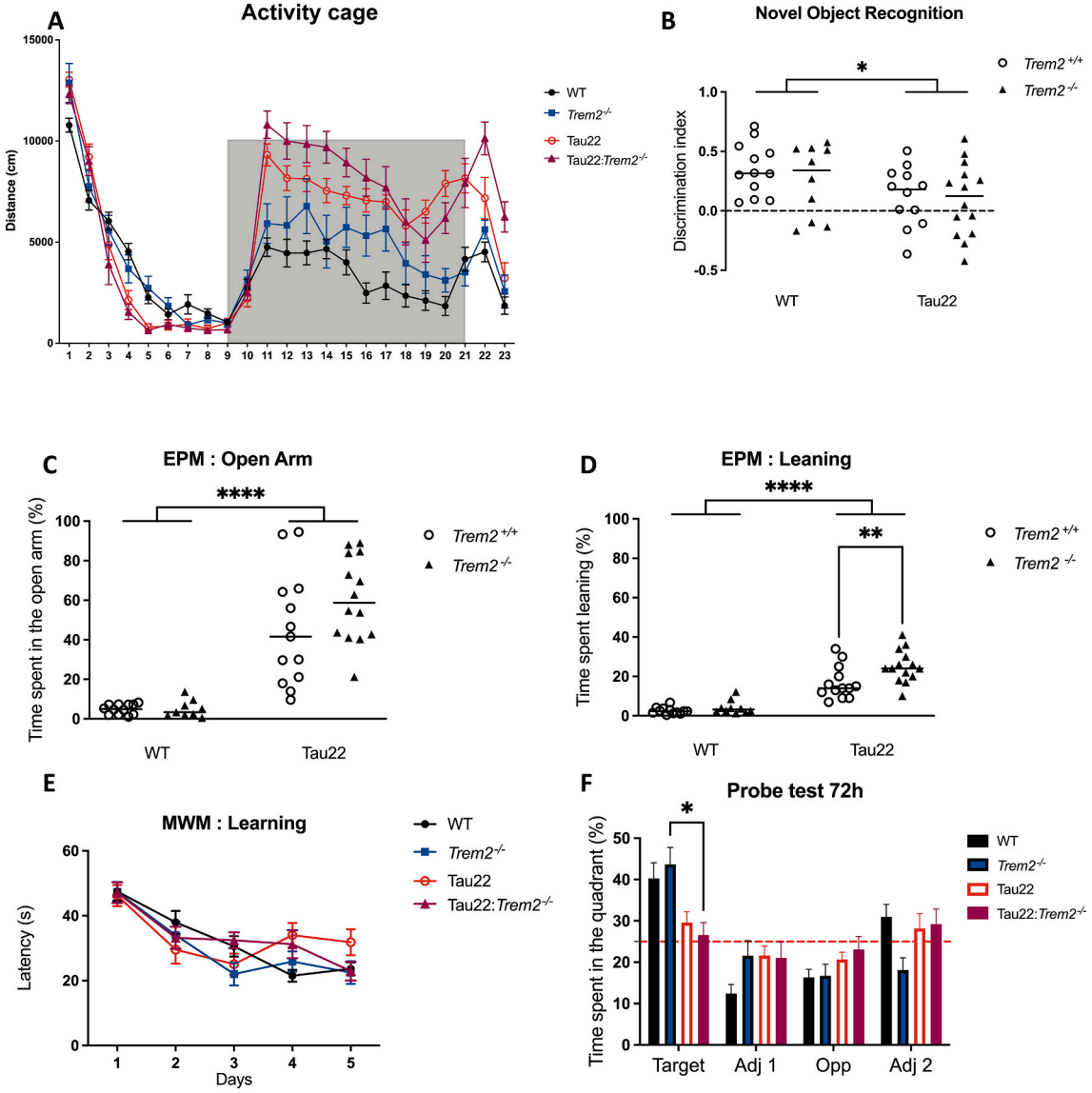

Fig. 6. *TREM2* deficiency did not induce any major behavioral alteration in Tau22 mice. (A) Distance traveled in the activity cage, hour by hour, during 23 h; MANOVA; F = 1,67 $p = 0,18$ for the day; F = 0,74 $p = 0,69$ for the night (grey area). (B) Discrimination index in the NOR test. (C) Fraction of time spent in the open arms of the elevated plus maze (EPM), Student *t*-test, $p = 0,06$. (D) Time spent leaning over the edge of open arms in the EPM, Student *t*-test, $p = 0,06$. (E) Escape latency for each day of the training phase of the the Morris water maze test (MWM) showing a significant effect of days but not of genotype (ANOVA repeated-mesures, F = 10,16 $p < 0,001$ between days and F = 0,0010 $p = 0,097$ between groups. (F) Percentage of time spent in each quadrant during the probe-test of the MWM performed 72 h after the last day of the training phase. Data are presented as mean ± SEM, n = 10–14/group, only males were used for behavioral assesment.

amyloid accumulation and lesions characteristic of tauopathy obtained by injection of patients' brain extracts into APPPS1–21 mice (Leyns et al., 2019). This study suggests that microglia could be a major player in the link between amyloid load and the progression of tauopathy. TREM2, by allowing the activation of microglia leading to the compaction of plaques (McQuade et al., 2020; Wang et al., 2016), would slow down this phenomenon. This in line with a recent study, which elegantly combines mouse models of amyloidosis and tauopathy with abrogation of the TREM2 function, and shows that TREM2 function restrains the triggering of Tau accumulation by ß-amyloid pathology (Lee, 2021). In this hypothesis, it appears rational to develop TREM2 agonists in order to explore new therapeutic avenues for AD (Cignarella et al., 2020; Price et al., 2020; Wang et al., 2020). On the other hand, the effects of TREM2 deficiency that we describe here, or those described by others (Leyns et al., 2017), in a context of pure tauopathy suggest that activating TREM2 could lead to a deleterious increase in microglial activation subsequent to tauopathy. To validate a therapeutic strategy targeting microglia and its TREM2 receptor, it therefore appears crucial to study its effects in pure models of either amyloid ß accumulation or tauopathy but also in mixed models presenting these two types of lesions.

CRediT authorship contribution statement

Audrey Vautheny: Investigation, Formal analysis, Visualization, Writing - original draft. **Charlotte Duwat:** Investigation, Formal analysis, Visualization, Writing - original draft. **Gwennaëlle Aurégan:** Investigation. **Charlène Joséphine:** Investigation. **Anne-Sophie Hérard:** Investigation. **Caroline Jan:** Investigation. **Julien Mitja:** Investigation. **Pauline Gipchtein:** Investigation. **Marie-Claude Gaillard:** Investigation. **Luc Buée:** Resources. **David Blum:** Resources, Writing - review & editing. **Philippe Hantraye:** Supervision. **Gilles Bonvento:** Supervision. **Emmanuel Brouillet:** Supervision. **Karine Cambon:** Conceptualization, Investigation, Writing - review & editing. **Alexis-Pierre Bemelmans:** Conceptualization, Investigation, Supervision, Formal analysis, Writing - original draft.

Declaration of Competing Interest

None.

Acknowledgements

This work was supported by a grant from Fondation Vaincre Alzheimer (grant LECMA-Vaincre Alzheimer #FR-15055), and by 'NeurATRIS ANR-11-INBS-0011', of the French Investissements d'Avenir Program run by the Agence Nationale pour la Recherche. DB and LB are supported by programs d'investissements d'avenir LabEx (excellence laboratory) DISTALZ (Development of Innovative Strategies for a Transdisciplinary approach to ALZheimer's disease) and ANR (ADORASTrAU ANR-18-CE16-0008 and CoEN 5008). AV received a doctoral fellowship from Université Paris-Saclay (Doctorate school 568 BIOSIGNE) and CD is the recipient of a doctoral fellowship from the "IDI 2017" project funded by the IDEX Paris-Saclay, ANR-11-IDEX-0003-02.

Appendix A. Supplementary data

Supplementary data to this article can be found online at https://doi.org/10.1016/j.nbd.2021.105398.

References

Allen, B., et al., 2002. Abundant tau filaments and nonapoptotic neurodegeneration in transgenic mice expressing human P301S tau protein. J. Neurosci. 22, 9340–9351.
Andorfer, C., et al., 2003. Hyperphosphorylation and aggregation of tau in mice expressing normal human tau isoforms. J. Neurochem. 86, 582–590.
Asai, H., et al., 2015. Depletion of microglia and inhibition of exosome synthesis halt tau propagation. Nat. Neurosci. 18, 1584–1593.
Augustinack, J.C., et al., 2002. Specific tau phosphorylation sites correlate with severity of neuronal cytopathology in Alzheimer's disease. Acta Neuropathol. 103, 26–35.
Bemiller, S.M., et al., 2017. TREM2 deficiency exacerbates tau pathology through dysregulated kinase signaling in a mouse model of tauopathy. Mol. Neurodegener. 12, 74.
Bouchon, A., et al., 2001. A DAP12-mediated pathway regulates expression of CC chemokine receptor 7 and maturation of human dendritic cells. J. Exp. Med. 194, 1111–1122.
Chatterjee, S., et al., 2018. Reinstating plasticity and memory in a tauopathy mouse model with an acetyltransferase activator. EMBO Mol. Med. 10.
Cignarella, F., et al., 2020. TREM2 activation on microglia promotes myelin debris clearance and remyelination in a model of multiple sclerosis. Acta Neuropathol. 140, 513–534.
Cipriani, G., et al., 2011. Alzheimer and his disease: a brief history. Neurol. Sci. 32, 275–279.
De Schepper, S., et al., 2020. Understanding microglial diversity and implications for neuronal function in health and disease. Dev. Neurobiol. In press.
Gratuze, M., et al., 2020. Impact of TREM2R47H variant on tau pathology-induced gliosis and neurodegeneration. J. Clin. Invest. 130, 4954–4968.
Guerreiro, R., et al., 2013. TREM2 variants in Alzheimer's disease. N. Engl. J. Med. 368, 117–127.
Hebert, L.E., et al., 2013. Alzheimer disease in the United States (2010-2050) estimated using the 2010 census. Neurology 80, 1778–1783.
Hopp, S.C., et al., 2018. The role of microglia in processing and spreading of bioactive tau seeds in Alzheimer's disease. J. Neuroinflammation 15, 269.
Ising, C., et al., 2019. NLRP3 inflammasome activation drives tau pathology. Nature 575, 669–673.
Jay, T.R., et al., 2015. TREM2 deficiency eliminates TREM2+ inflammatory macrophages and ameliorates pathology in Alzheimer's disease mouse models. J. Exp. Med. 212, 287–295.
Jay, T.R., et al., 2017. Disease progression-dependent effects of TREM2 deficiency in a mouse model of Alzheimer's disease. J. Neurosci. 37, 637–647.
Jiang, T., et al., 2014. Upregulation of TREM2 ameliorates neuropathology and rescues spatial cognitive impairment in a transgenic mouse model of Alzheimer's disease. Neuropsychopharmacology 39, 2949–2962.
Jiang, T., et al., 2015. Silencing of TREM2 exacerbates tau pathology, neurodegenerative changes, and spatial learning deficits in P301S tau transgenic mice. Neurobiol. Aging 36, 3176–3186.
Jonsson, T., et al., 2013. Variant of TREM2 associated with the risk of Alzheimer's disease. N. Engl. J. Med. 368, 107–116.
Keren-Shaul, H., et al., 2017. A unique microglia type associated with restricting development of Alzheimer's disease. Cell 169 (1276–1290), e17.
Krasemann, S., et al., 2017. The TREM2-APOE pathway drives the transcriptional phenotype of dysfunctional microglia in neurodegenerative diseases. Immunity 47 (566–581), e9.
Laurent, C., et al., 2016. A2A adenosine receptor deletion is protective in a mouse model of Tauopathy. Mol. Psychiatry 21, 97–107.
Laurent, C., et al., 2017. Hippocampal T cell infiltration promotes neuroinflammation and cognitive decline in a mouse model of tauopathy. Brain 140, 184–200.
Laurent, C., et al., 2018. Tau and neuroinflammation: what impact for Alzheimer's Disease and Tauopathies? Biom. J. 41, 21–33.
Lee, S.H., et al., 2021. Trem2 restrains the enhancement of tau accumulation and neurodegeneration by beta-amyloid pathology. Neuron 109, 1283–1301.
Leyns, C.E.G., et al., 2017. TREM2 deficiency attenuates neuroinflammation and protects against neurodegeneration in a mouse model of tauopathy. Proc. Natl. Acad. Sci. U. S. A. 114, 11524–11529.
Leyns, C.E.G., et al., 2019. TREM2 function impedes tau seeding in neuritic plaques. Nat. Neurosci. 22, 1217–1222.
Liddelow, S.A., et al., 2017. Neurotoxic reactive astrocytes are induced by activated microglia. Nature 541, 481–487.
Mak, K.S., et al., 2011. PU.1 and haematopoietic cell fate: dosage matters. Int. J. Cell Biol. 2011, 808524.
Maphis, N., et al., 2015. Reactive microglia drive tau pathology and contribute to the spreading of pathological tau in the brain. Brain 138, 1738–1755.
McQuade, A., et al., 2020. Gene expression and functional deficits underlie TREM2-knockout microglia responses in human models of Alzheimer's disease. Nat. Commun. 11, 5370.
Parhizkar, S., et al., 2019. Loss of TREM2 function increases amyloid seeding but reduces plaque-associated ApoE. Nat. Neurosci. 22, 191–204.
Price, B.R., et al., 2020. Therapeutic Trem2 activation ameliorates amyloid-beta deposition and improves cognition in the 5XFAD model of amyloid deposition. J. Neuroinflammation 17, 238.
Puighermanal, E., et al., 2009. Cannabinoid modulation of hippocampal long-term memory is mediated by mTOR signaling. Nat. Neurosci. 12, 1152–1158.
Sayed, F.A., et al., 2018. Differential effects of partial and complete loss of TREM2 on microglial injury response and tauopathy. Proc. Natl. Acad. Sci. U. S. A. 115, 10172–10177.
Schindowski, K., et al., 2006. Alzheimer's disease-like tau neuropathology leads to memory deficits and loss of functional synapses in a novel mutated tau transgenic mouse without any motor deficits. Am. J. Pathol. 169, 599–616.
Serrano-Pozo, A., et al., 2011. Neuropathological alterations in Alzheimer disease. Cold Spring Harb. Perspect. Med. 1, a006189.

Stancu, I.C., et al., 2019. Aggregated Tau activates NLRP3-ASC inflammasome exacerbating exogenously seeded and non-exogenously seeded tau pathology in vivo. Acta Neuropathol. 137, 599–617.
Turnbull, I.R., et al., 2006. Cutting edge: TREM-2 attenuates macrophage activation. J. Immunol. 177, 3520–3524.
Ulland, T.K., et al., 2017. TREM2 maintains microglial metabolic fitness in Alzheimer's disease. Cell. 170 (649–663), e13.
Van der Jeugd, A., et al., 2011. Hippocampal tauopathy in tau transgenic mice coincides with impaired hippocampus-dependent learning and memory, and attenuated late-phase long-term depression of synaptic transmission. Neurobiol. Learn. Mem. 95, 296–304.
Van der Jeugd, A., et al., 2013a. Observations in THY-Tau22 mice that resemble behavioral and psychological signs and symptoms of dementia. Behav. Brain Res. 242, 34–39.
Van der Jeugd, A., et al., 2013b. Progressive age-related cognitive decline in tau mice. J. Alzheimers Dis. 37, 777–788.
Wang, Y., et al., 2015. TREM2 lipid sensing sustains the microglial response in an Alzheimer's disease model. Cell 160, 1061–1071.
Wang, Y., et al., 2016. TREM2-mediated early microglial response limits diffusion and toxicity of amyloid plaques. J. Exp. Med. 213, 667–675.
Wang, S., et al., 2020. Anti-human TREM2 induces microglia proliferation and reduces pathology in an Alzheimer's disease model. J. Exp. Med. 217.
Webers, A., et al., 2019. The role of innate immune responses and neuroinflammation in amyloid accumulation and progression of Alzheimer's disease. Immunol. Cell. Biol. 98, 28–41.
Yoshiyama, Y., et al., 2007. Synapse loss and microglial activation precede tangles in a P301S tauopathy mouse model. Neuron 53, 337–351.
Yuan, P., et al., 2016. TREM2 haplodeficiency in mice and humans impairs the microglia barrier function leading to decreased amyloid compaction and severe axonal dystrophy. Neuron 92, 252–264.